NASA TECHNICAL MEMORANDUM

NASA TM X-71873

NASA TM X-71873

DESIGN AND EVALUATION OF A 3 MILLION DN SERIES-HYBRID THRUST BEARING

by Herbert W. Scibbe
Lewis Research Center
Cleveland, Ohio 44135

and

Leo W. Winn and Martin Eusepi
Mechanical Technology Incorporated
Latham, New York

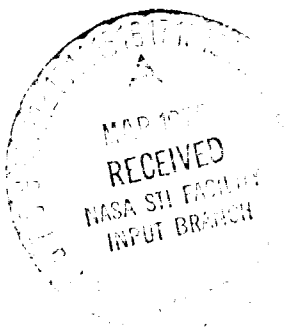

TECHNICAL PAPER to be presented at
Spring Lubrication Symposium sponsored
by the American Society of Mechanical Engineers
Atlanta, Georgia, May 24-26, 1976

NASA TECHNICAL MEMORANDUM

NASA TM X-71873

NASA TM X-71873

DESIGN AND EVALUATION OF A 3 MILLION DN SERIES-HYBRID THRUST BEARING

by Herbert W. Scibbe
Lewis Research Center
Cleveland, Ohio 44135

and

Leo W. Winn and Martin Eusepi
Mechanical Technology Incorporated
Latham, New York

TECHNICAL PAPER to be presented at
Spring Lubrication Symposium sponsored
by the American Society of Mechanical Engineers
Atlanta, Georgia, May 24-26, 1976

DESIGN AND EVALUATION OF A 3 MILLION DN SERIES-HYBRID THRUST BEARING

by

Herbert W. Scibbe
NASA-Lewis Research Center

and

Leo W. Winn and Martin Eusepi
Mechanical Technology Incorporated

E-8646

ABSTRACT

The design and experimental evaluation of a series-hybrid thrust bearing, consisting of a 150-mm ball bearing and a centrifugally actuated, conical, fluid-film bearing is presented. Tests were conducted up to 16 000 rpm and at this speed an axial load of 15568 N (3500 lb) was safely supported by the hybrid bearing system. Through the series-hybrid bearing principle, the effective ball bearing speed was reduced to approximately one-half of the shaft speed. A speed reduction of this magnitude would result in a ten-fold increase in the ball bearing fatigue life. A successful evaluation of fluid-film bearing lubricant supply failure was performed repeatedly at an operating speed of 10 000 rpm. A complete and smooth changeover to full-scale ball bearing operation was effected when the oil supply to the fluid-film bearing was cut off. Reactivation of the fluid-film oil supply system produced a flawless return to the original mode of hybrid operation.

INTRODUCTION

An important consideration in the application of ball bearings to high-speed rotating machinery is the improvement of fatigue life. The

use of low mass hollow or drilled balls in high-speed bearings to reduce contact stress and thereby improve fatigue life, has been demonstrated with limited success in several experimental programs. [1-5][1] Another method for improving fatigue life of a ball bearing is to reduce its rotational speed by coupling it in series with a fluid-film bearing. This arrangement called the series-hybrid bearing, is shown in Fig. 1. In the series-hybrid bearing, each bearing component carries the full thrust load at its respective speed. The inner fluid-film bearing member rotates with the shaft at full speed. The mating fluid-film bearing member rotates with the ball bearing inner race at some fraction of the shaft speed. The outer race of the ball bearing is mounted in a stationary housing. Oil to pressurize the fluid-film bearing and lubricate the ball bearing is fed through the hollow shaft.

At low speed the inner and mating intermediate fluid-film bearing members rotate together at the same speed; however as shaft speed increases the fluid-film bearing lifts off at its pad, due to the hydrostatic pressure developed by the centrifugal force of the lubricant fed through the shaft. At lift off, there is a differential in speed between the inner member of the fluid-film bearing and intermediate member attached to the inner race of the ball bearing. This speed differential results in a lower speed for the ball bearing and thereby reduces ball centrifugal force (and thus contact stress) at the outer race. Up to 33 percent reduction in ball bearing inner-race speed has been successfully demonstrated in a test program, [6] where in a combination self-acting journal and hydrostatic thrust fluid-film bearing was coupled to a 75-millimeter-bore ball bearing.

[1]Numbers in [brackets] designate references at end of paper.

The series-hybrid bearing has several advantages when compared to both the hollow and drilled ball bearing concepts at DN (bearing bore in mm times shaft shaft speed in rpm) values from 3 to 4 million. Two of these advantages, a greater bearing life improvement potential and the built-in fail-safe feature of the backup ball bearing, make the series-hybrid bearing a very attractive high-speed bearing concept.

The objective of this investigation was to design, fabricate, and test a series-hybrid bearing configuration over a range of running conditions. An optimally configured conical hydrostatic fluid-film bearing coupled to a 150 millimeter bore angular contact, split-inner ring ball bearing was specified for the series-hybrid bearing configuration. The fluid-film bearing was optimally designed with a low torque-rotational speed characteristic to match that of the ball bearing at 20 000 rpm shaft speed. A 30 to 40 percent reduction in ball bearing inner race speed at a 3 million DN equivalent shaft speed was predicted for the series-hybrid bearing design based on the analytical study of Ref. [7].

NOMENCLATURE

C_d Orifice discharge coefficient

C_1 Dimensionless laminar friction coefficient, $4h_L fr/h_p$

C_2 Dimensionless turbulent friction coefficient, $0.026/fr[\rho R_1(\omega_s - \omega_b)h_p/\mu]^{0.75} h_L/h_p$

d Orifice diameter

F Thrust load

$\overline{F}$ Dimensionless thrust load, $F/(\pi p R_1^2)$

fr Fraction of area between R_2 and R_3 occupied by hydrostatic pockets

h_L Fluid-film thickness

h_p Hydrostatic pocket depth

k Fluid-film resistance ratio, $(2\rho p_s/9)^{0.5} h_L^3 \sin\theta / C_d n d^2 \mu \left[1/\ln X_2 + 1/\ln(X_4/X_3)\right]$

M_L Land fluid-film bearing torque

$\overline{M}_L$ Dimensionless land fluid-film bearing torque, $2M_L h_L \sin\theta / \pi\mu(\omega_s - \omega_b)R_1^4$

M_p Pocket fluid-film bearing torque

$\overline{M}_p$ Dimensionless pocket fluid-film bearing torque, $2M_p h_L \sin\theta / \pi\mu(\omega_s - \omega_b)R_1^4$

M_t Total fluid-film bearing torque, $M_L + M_p$

n Number of feeding orifices

p Pocket pressure

$\overline{p}$ Dimensionless pocket pressure, p/p_s

p_s Supply pressure

Q Fluid flow

$\overline{Q}$ Dimensionless fluid flow, $6\mu Q / \pi p h_L^3 \sin\theta$

R_0 Radial location of feeding orifices

R_1 Inner radius of inner land

R_2 Outer radius of inner land

R_3 Inner radius of outer land

R_4 Outer radius of outer land

X_2 R_2/R_1

X_3 R_3/R_1

X_4 R_4/R_1

θ Half-angle of conical hydrostatic bearing

μ Fluid viscosity

ρ Fluid density

ω_b Ball bearing speed

ω_c Bearing cage speed

ω_s Shaft speed

ANALYTICAL DESIGN

Series-Hybrid Thrust Bearing Design

A characteristic of operation of the series-hybrid system is that the friction torque causing ball bearing rotation is the torque transmitted through the fluid-flim bearing. As each component rotates under the same applied thrust load, the speed of each is dependent upon the torque-speed relation of that bearing component. Success of the series-hybrid bearing concept in reducing the speed of the ball bearing depends on the fluid-film bearing operating at the same low torque at a fraction of the shaft speed, The series-hybrid bearing design selected for this investigation was based on a shaft speed of 20 000 rpm and thrust load of 17 800 newtons (4000 lb). These conditions are representative of a mainshaft ball bearing in a gas turbine engine operating at maximum thrust load to simulate aircraft take-off conditions. Off design performance at 10 000 and 15 000 rpm and 4450 newton (1000 lb) thrust load were also specified for the series-hybrid bearing, as these are representative of engine cruise conditions.

Fluid-Film Bearing Design

An oil-fed fluid-film bearing having low torque-rotational speed characteristic was required to match the torque of the ball bearing and thereby obtain an appreciable reduction in ball bearing speed. Although thrust was the primary load designed for in this application, the bearing should also have radial load capacity. To avoid complexity and reduce

the friction of separate thrust and journal bearings, a conical hydrostatic bearing was selected. A schematic of the conical hydrostatic bearing, indicating the location of bearing land and pocket radii, is shown in Fig. 2. Fluid is introduced at the shaft center-line (fig. 2(a)) and is fed radially to orifice flow restricters, at radius R_0, which provide pressure compensation for potential misalinement and varying loads. The hydrostatic pressure available for load capacity is that developed at radius R_0 because of centrifugal effects. After the fluid (oil) passes through the compensating orifice, a pressure p is available in the hydrostatic pockets to resist a thrust load, F. (Symbols are defined in the Nomenclature.) The required pressure area is determined by the thrust load and the bearing must carry at supply pressure, p_s.

The design of the fluid-film bearing must be optimized so that it yields minimum friction torque at the specified design speed and load conditions. Geometric dimensions and oil feeding arrangements were to be determined for a hydrostatic bearing that satisfy the following conditions;

1. An envelope size with an outer radius (R_4) equal to or less than 84.8 millimeters (3.34 in.) and an inner radius (R_1) equal to or greater than 71.4 millimeters (2.81 in.).

2. A bearing conical half-angle equal to 45 degrees.

3. A design oil viscosity of 5.5×10^{-3} newtons per second per square meter (8×10^{-1} lb-sec/in^2) and oil density of 9.4×10^2 kilograms per cubic meter (0.34 lb/in^3) at a temperature of 367° K (200° F).

4. At the design speed of 20 000 rpm and design load of 17 800 newtons (4000 lb) the fluid-film bearing friction torque shall be a minimum

5. At 20 000 rpm and a load of 4450 newtons (1000 lb) the oil flow rate shall be 37.9 liters per minute (10 gpm) maximum.

Design optimization of a conical hydrostatic fluid-film bearing was first performed in [8] based on a computer solution. A similar optimized bearing design procedure was followed in this effort. Selection of the bearing configuration and details of the design procedure used are given in the appendix and also in [9].

Selected fluid-film bearing design. - The design procedure followed in the appendix yielded optimized bearing configuration. Other considerations in selecting a finalized optimal bearing configuration were; (1) bearing stiffness at the design load and speed and at off-design conditions, (2) oil flow rates sufficient to provide adequate film thickness, and (3) bearing friction torques over the range of speeds and loads. Dimension and operating parameters of the selected bearing design given in the appendix are also shown on Fig. 3. Bearing load and flow as a function of film thickness for a $\bar{p} = 0.3$ at the design speed of 20 000 rpm is shown in Fig. 3. It appears the bearing has good stiffness in the design load range and the flow rates are within the range specified in (5) above. Fig. 3 also shows the bearing load and flow values as a function of film thickness at shaft speeds of 10 000 and 15 000 rpm.

The axial stiffness of the selected bearing are plotted in Fig. 4 for speeds of 10 000, 15 000, and 20 000 rpm. These stiffnesses were obtained by numerical differentiation of the $F - h_L$ data presented in Fig. 3.

Ball Bearing Configuration

The ball bearing component specified for the series-hybrid bearing was a 150-millimeter bore split-inner ring design. The bearing had a

radial clearance of 0.107 to 0.142 millimeter (0.0042 to 0.0056 in.) with a nominal contact angle of 30 degrees. Ball and race material was AISIM-50CEVM steel with a Rockwell hardness of 60 to 63. Cage material was AISI4340 steel with 0.025 to 0.051 millimeter (0.001 to 0.002 in.) thick silver plate. Complete bearing specifications are given in [5].

The measured torque values for the ball bearing from [5] at 8900 and 17 800 newtons (2000 and 4000 lb) thrust load are given in table I for inner-race speeds from 6670 to 20 000 rpm. These torque values which increase with speed, as was anticipated, were used to calculate the differential speed between the fluid-film and ball bearing components of the series-hybrid bearing. The ball bearing stiffness ranged from 6.98 newtons per centimeter (3.7×10^{-5} lb/in) at 17 800 newtons (4000 lb) thrust load and 20 000 rpm to 1.58 newtons per centimeter (0.9×10^{-5} lb/in) at 4450 newton (1000 lb) load and 10 000 rpm. These stiffness values were used in the rotor dynamic stability determination for the series-hybrid bearing over the entire test-speed range.

Predicted Series-Hybrid Bearing Performance

Once the torque characteristics of the fluid-film bearing and ball bearing components were known, the performance characteristics of the combined hybrid bearing could be calculated. The effects of speed and load on fluid-film bearing flow and film thickness have been discussed previously in the fluid-film bearing design section. Other important parameters to be determined for the hybrid bearing design were: (1) the differential speed between the ball and fluid-film bearing components, and (2) the net benefits of the speed differentials in terms of ball bearing life and bearing power loss.

Determination of Differential Speed

The split between the shaft speed and that of the ball bearing inner race can be determined from a crossplot of ball bearing and fluid-film bearing torques as a function of ball bearing to shaft speed ratio ω_b/ω_s. The speed ratio data (ω_b/ω_s) for 8900 and 17 800 newtons (2000 and 4000 lb) thrust loads at the three shaft speeds is given in table II. The crossplot of this torque data is shown in Fig. 5 for a test shaft speed of 20 000 rpm. Note that the ball bearing torque at 8900 newtons (2000 lb) is approximately one-half that at 17 800 newtons (4000 lb). This high degree of torque dependence on load is more indicative of Coulomb friction rather than of friction existing in well lubricated bearings operating on an elastohydrodynamic film. Along the 17 800 and 8900 newton (4000 and 2000 lb) load curves for the fluid-film bearing in Fig. 5, the points of equal torque are shown at the intersection of the ball bearing axial load curves of 17 800 and 8900 newtons (4000 and 2000 lb). At these intersection points the ball bearing inner-race speeds are 46 and 61 percent, respectively, of the shaft speed of 20 000 rpm.

The hybrid bearing should be capable of supporting 17 800 newtons (4000 lb) at shaft speeds of 20 000 and 15 000 rpm At 10 000 rpm, the load carrying capacity drastically decreases because of the reduction in the pressure due to inertia forces At this speed, the load corresponding to a 0.0254 millimeter (1 mil) film thickness is 11 900 newtons (2670 lb) see Fig. 3.

Net Benefits of Ball Bearing Speed Reduction

The combination of high thrust load and high speed severely limits the ball bearing life. This limitation is difficult, and in some cases

impossible to overcome with mere changes in ball bearing design and materials. The series hybrid bearing arrangement brings about a net reduction in ball bearing speed and consequently mitigates the limitations imposed by the severe operating conditions. A comparison of the fatigue life of the ball bearing operating at 20 000 rpm within the specified load range of 8900 to 17 800 newtons (2000 to 4000 lb) indicates that bearing fatigue life improvement is more than tenfold when going from a single bearing to the series-hybrid bearing configuration. For example, at 17 800 newton (4000 lb) thrust load, the B_{10} life is increased from 100 hours to 1150 hours. The B_{10} life was calculated based on air melted race and ball material without elastohydrodynamic film or material improvement factors considered.

The greatest disadvantage of the hybrid bearing lies in its flow requirements. The flow consumption of the hybrid bearings at 20 000 rpm and 17 800 newtons (4000 lb) load is calculated to be 28.4 liters per minute (7.5 gpm) for the fluid-film bearing plus 4 54 liters per minute (1.2 gpm) for the ball bearing alone at the above conditions of operation. The increased flow, however, does not represent as great an obstacle to operation at high speeds and high loads as that presented by the inherent ball bearing fatigue life limitations

A thermal and elastic deformation analysis were performed on the selected series-hybrid design The thermal analysis indicated relatively low axial and radial thermal gradients for the fluid-film bearing runner and stater. A maximum temperature rise of 11° K (20° F) for an inlet oil temperature of 367° K (200° F) indicated that the ball and fluid-film bearing lubricant flows are adequate and no temperature gradients exist that will adversely affect the series-hybrid bearing operation

The calculated results of the distortion analysis indicated that a nominal radial growth and relative rotation between the primary and intermediate rotor faces of the fluid-film bearing occurs. The net effect, however, results in less than 2.54×10^{-3} millimeter (0.0001 in.) net loss in film thickness at the bearing outer edge. Based on these small deformations at the bearing surfaces the degradation in fluid-film bearing performance is negligible.

TEST APPARATUS AND INSTRUMENTATION

Test-head assembly. - The major components of the series hybrid test head are shown in Fig. 6. The three bearing test spindle was directly coupled to and driven by 100 HP DC motor through a 6.34 to 1 step-up gear box. Shaft speed was continuously variable from 1000 to 20 000 rpm. Thrust load for the hybrid bearing assembly was provided by a hydraulic cylinder ram that pushed on the end cover of the test head (fig. 6). A more detailed discussion of the test head assembly can be found in [10].

Test instrumentation. - Film thickness between the runner and intermediate member of the fluid-film bearing was measured by eddy current position sensors mounted in pairs in holding blocks as shown in Fig. 6. Four pairs of these probes were mounted every 90 degrees around the periphery of the bearing. To provide for temperature compensation and obtain a true calibration value, each probe contains an iron-constantan thermocouple. Four iron-constantan thermocouples, spaced 90 degrees apart in the bearing housing at the axial mid-point of the ball bearing, were used to measure outer race temperature. A single I-C thermocouple, positioned at the top of the bearing housing in Fig. 6, was used to measure oil discharge temperature.

The magnetic pickup shown was used to measure intermediate bearing member speed, whereas the eddy current sensing probe shown above it was used to measure ball bearing cage speed.

Additional test instrumentation not shown in Fig. 6 were (1) two (2) float type flow meters to measure fluid-film and ball bearing oil flow rates, an iron-constantan thermocouple in each line provided oil inlet temperature values; (2) pressure gages to indicate fluid-film bearing oil supply pressure and load cylinder pressure to determine applied axial load; and (3) a magnetic pickup at the motor end of the test spindle to measure shaft speed.

Torque on the series-hybrid test assembly was measured through torque arms on opposite sides of the bearing housing. The arm contained balls that transmitted torque by point contact to deflection beams instrumented with strain gages. Beam deflection is proportional to strain gage voltage output that was recorded on a strip chart. The beams were allowed to deflect a limited amount before they met solid stops.

Lubricant supply system. - A skid mounted lubricant system provided adequate synthetic lubricant to the fluid-film and ball bearings at pressures to 8.60×10^5 N/m^2 (125 psi), at flow rates to 9.25×10^{-4} m^3/sec (13 gpm) at inlet oil temperatures to 422° K (300° F). The lubricant used in the series-hybrid bearing tests was a type II ester manufactured to MIL-L 23699 specifications. A second pumping unit, designed to supply only mineral oil, was capable of providing $6.31 \cdot 10^{-3}$ m^3/sec (10 gpm) at $1.04 \cdot 10^1$ N/m^2 (1500 psi) pressure at temperatures not exceeding 336° K (145° F). The lubricant used for the fluid-film bearing tests was an SAE-10 mineral oil

TEST PROCEDURE

The first test run was performed to establish the system's characteristics at gradually increasing levels of load and speed. The initial conditions set were: (1) thrust load, 225 newtons (500 lb); (2) ball bearing oil flow rate, 6.31×10^{-5} m^3/sec (1.0 gpm); (4) inlet oil temperature, 367° K (200° F) of type II ester oil (MIL-L 23699). At these static conditions, the shaft rotational speed was gradually increased to 2200 rpm and held until thermal equilibrium within the test head was established. After thermal stability was obtained, rotor speed and axial load were increased sequentially until 10 000 rpm and a 4480 newton (1000 lb) load was reached.

At a shaft speed of 2200 rpm, the fluid-film bearing still remained inoperative and the speed of the intermediate member was equal to that of the shaft. At about 3500 rpm, the fluid-film bearing surfaces suddenly parted, establishing a separating oil film between the shaft and intermediate member. Simultaneously, with the parting of the fluid-film bearing surfaces, the ball bearing speed dropped to 42 percent of the shaft speed. This was observed on the intermediate speed indicator, as well as on the bearing cage speed indicator.

The oil supplied to the center of the test shaft was introduced into the radial passages of the inner fuild-film bearing member. The oil pressure was read at the point where the oil entered the end cover (see fig. 6). The capability of supplying large volumes of pressurized oil allowed checking the fluid-film bearing behavior not only at lower speed, but at pressures simulating those that were centrifugally developed at higher speeds. Furthermore, the direct readings of the pressure inside the shaft provided a positive identification of a continual presence of oil in this area. As

long as the flow to the fluid-film bearing was satisfied, the inner shaft volume remained at a positive pressure. As soon as that pressure reached zero, it was determined that the flow requirements to the fluid-film bearing had reached the upper supply limit and no additional load capacity could be developed.

A test sequence to establish the performance of the fluid-film bearing component separately, was run. The remaining test sequences provided data for the performance of the series-hybrid bearing operational and fail safe tests.

The test plan called for the fluid-film bearing evaluation to be performed using a type II ester (MIL-L-23699) lubricant. Preliminary runs with the high pressure lubricant supply system disclosed that this system was not capable of operating on the synthetic ester type oil at temperatures of (367° K) (200° F). As a result of this restriction, the tests of the fluid-film bearing were performed using a SAE-10 mineral oil. The hybrid bearing tests were conducted using the specified MIL-L-23699 lubricant.

RESULTS AND DISCUSSION

Fluid-film Bearing Tests

The fluid-film bearing tests were performed to establish the load carrying capacity of this component of the series hybrid bearing under hydrostatic action when oil was supplied from an external source. The tests consisted of operating the fluid-film bearing at rotor speeds of 0, 2000, 4000, 6000, and 8000 rpm. An SAE-10 oil was used at supply pressures of 251×10^4, 569×10^4, and 1010×10^4 N/m^{-2} (364, 825, and 1465 psi) which corresponded to pressures that would be developed centrifugally at shaft speeds of 10 000, 15 000, and 20 000 rpm. Applied

load was varied between 2220 and 17 800 newtons (500 and 4000 lb) depending upon the load carrying capability of the oil film at the specific simulated shaft speeds. Results of the fluid-film bearing tests are shown in Fig. 7. Of primary interest were the effects of speed, load, and hydrostatic supply pressure on the film thickness and oil flow rates. Comparison between the experimental and analytical results indicated several important differences. Figure 7 shows the film thickness as a function of load (or bearing stiffness) for the three hydrostatic supply pressures. The experimental film thickness shown at each load was averaged from values obtained at rotor speeds from 0 to 8000 rpm. The experimental curve drawn through the points appears to have the same slope as the theoretical curves for 0, 4000, and 8000 rpm, shown on the right. However, for a given thrust load the measured film thickness did not increase with increasing rotor speed in every case, as shown for the theoretical curves. This phenomenon is in contrast to normally expected behavior where increasing speed and resulting centrifugal pressure augmentation increase the load carrying capacity, as indicated by the analytical results.

Reasons for observed differences between the experimental and analytical values of film thickness are discussed in more detail in the CONCLUDING REMARKS section of this report. It can be noted here that the effect of speed on fluid-film bearing load capacity is more pronounced at low supply pressures (fig. 7(a)) than at the higher supply pressures (fig. 7(c)) where the augmenting action of the centrifugal pumping forces represent a smaller fraction of the load carrying capacity.

The fluid-film bearing test data indicates ample load carrying capacity at high speeds of operation with reasonable oil flow rates. Loads of

6672 newtons (1500 lb) can be sustained at equivalent DN values of 1.5 million (10 000 rpm), with flows not exceeding 3.46×10^{-4} m^3/sec (5.5 gpm). At equivalent DN values of 2.25 million (15 000 rpm) the load carrying capacity can reach 13 250 newtons (3000 lb) with the flow not exceeding 4.73×10^{-4} m^3/sec (7.5 gpm) and at equivalent of 3 million DN (20 000 rpm), 17 792 newtons (4000 lb) can be safely supported with flow rates less than 5.93×10^{-4} m^3/sec (9.5 gpm).

Series Hybrid Bearing Tests

Successful tests were conducted with the series-hybrid bearing over the speed range from 5000 to 15 000 rpm and at thrust loads from 4450 to 13 240 newtons (1000 to 3000 lb) using MIL-L-23699 oil. Test results are presented in table III, and the flow and torque measurement data are shown in Figs. 8 and 9, respectively.

The film thickness data for the hybrid tests showed values consistently lower than predicted. Examination of the individual probe readings indicates that some misalignment occurred as the test conditions were varied, but the apparent low film thickness readings were felt to be primarily caused by the same effects noted previously for the fluid-film bearing tests.

Results of the flow (fig. 8) and torque data (fig. 9) from the hybrid tests showed good correlation with theoretically predicted values. Additionally, the speed ratio (ω_b/ω_s) or the split between the ball bearing inner-race and shaft speeds was better than predicted. For example, at 8900 newton (2000 lb) thrust load and 10 000 and 15 000 rpm the speed ratios were 0.495 and 0.475, respectively (table III). These values were lower than those predicted, since table II shows speed ratio values of 0.590 and 0.600 at these bearing operating conditions.

The series hybrid test sequence had to be modified somewhat after the 4450 newton (1000 lb) thrust load tests had been run. It became apparent that to remain within the supply capability of the pump, the higher speed runs would have to be made at higher axial loads. As a result 6670 and 8900 newton (1500 and 2000 lb) thrust loads were added to the test program. Also a 13 350 newton (3000 lb) load was substituted for the 4450 newton (1000 lb) load at 15 000 rpm.

At the conclusion of the 15 000 rpm, 13 350 newton (3000 lb) test point, the load was raised to 15 600 newtons (3500 lb) and the rotor speed was slowly increased. At approximately 16 500 rpm, the residual pressure supplying the fluid-film bearing reached zero, indicating that the maximum flow rate of the lubricant pumping system had been achieved. Therefore, no attempt was made to run the 20 000 rpm tests.

Fail-Safe Tests

Prior to final disassembly, an oil system failure was simulated (fail-safe test) at a speed of 10 000 rpm and a 4450 newton (1000 lb) axial load, by stopping the oil flow to the fluid-film bearing several times. Each time the oil flow to the fluid bearing was terminated, the ball bearing inner race accelerated quickly to the shaft speed level without any audible changes in the system performance. Similarly, the restoration of oil flow to the fluid-film bearing with the shaft speed maintained at 10 000 rpm resulted in fluid-film bearing activation and a reduction of the ball bearing speed to 43 percent of the shaft speed - an excellent speed split. In these oil system failure tests, the ball bearing temperature would stabilize at 378° K (220° F) when the fluid-film bearing was activated. At the time of oil shutdown to the fluid-film bearing, the temperature of the outer race

of the ball bearing rose to 401° K (265° F). This increase in outer race temperature was mainly due to the increase in the effective ball bearing speed.

Tear-down and inspection of the bearing after the fail-safe series of tests showed the fluid-film bearing and ball bearing to be in excellent condition. The bearing surfaces of the runner and the intermediate member had circumferential scratches and burnishes, but these were not of sufficient magnitude to affect bearing performance.

CONCLUDING REMARKS

Generally, the independent fluid-film bearing tests indicated good performance under all test conditions, but with some anomalies.

It was shown experimentally, that at several different thrust loads, an increase in rotor speed at constant lubricant supply pressure produced a decrease in the measured bearing clearance. This result was contrary to the analytical predictions, where an increase in speed should produce an increase in film thickness. In addition, the average experimental values of film thickness measured at any individual supply pressure over the test range, were consistently smaller than the predicted values and always by a nearly similar amount of 1.27×10^{-5} meter (5.0×10^{-4} in.)

A plausible explanation for both of the above observed effects, i.e., film thickness reduction with speed, as opposed to analytically predicted film thickness increase, and the generally reduced overall measured film thickness level, lies in the methods used to measure temperature.

The oil discharge temperature (oil leaving the bearing) is measured by thermocouples, each attached to a probe bracket. This temperature is also used to compensate for thermal errors inherent in the performance

of the proximity probes. These thermocouples are surface mounted with their junction exposed to both the exit oil spray and the metal temperature of the probe holder. Since the probe holder is firmly attached to the housing, the heat conduction away from the probe holder will tend to lower the apparent temperature indicated by the thermocouple.

The probe calibration curves generally showed a zero shift of about 5.08×10^{-6} meters per ^{o} K (1×10^{-4} in. per ^{o} F) with no thermal effect on the calibration surve slope. Thus, should the measured temperature reading be in error by 2.5^{o} K (5^{o} F), an observed error of 1.27×10^{-5} meter (5.0×10^{-4} in.) between the measured and calculated film thickness values could be easily explained. Furthermore, higher relative velocities within the fluid-film bearing, caused by increased rotor speed, will generate higher levels of heat within the bearing clearance, thereby also exaggerating this thermal effect.

The speed splits obtained in the tests are obviously more favorable than those originally anticipated by analysis. The split, however, is in a large measure a function of the ball bearing torque. The ball bearing torque values employed in the original analysis were those obtained on test, as reported in [5]. These tests were performed with normal ball bearing mounts. In the series hybrid bearing arrangement, the oil emanating from the fluid-film bearing imparts an additional churning torque on the ball bearing inner race or the intermediate member. This can increase the ball bearing torque value and result in a more favorable split. That fact may be utilized to the designer's advantage in future applications.

SUMMARY OF RESULTS

A series-hybrid thrust bearing configuration consisting of a conical

hydrostatic fluid-film bearing and a 150-millimeter-bore ball bearing was designed and tested. A type II ester oil was used in the fluid-film bearing to develop the hydrostatic load capacity by centrifugal inertia force and to lubricate the ball bearing. The study produced the following results:

1. Tests were conducted up to 16 500 rpm (2.5 million equivalent DN value) and an axial load of 15 600 newtons (3500 lb) was safely supported by the series bearing system. Through the employment of the series hybrid bearing principle, it was possible to reduce the effective bearing speed to approximately one-half of the shaft speed. A reduction of this magnitude can result in a ten fold increase in ball bearing fatigue life. The experimental performance of the series hybrid has proven the series hybrid principle to be a viable means of reducing DN levels of large ball bearings operating in high-speed, high-load systems.

2. A sucessful evaluation of lubricant supply failure (fail-safe tests) was performed at an operating speed of 10 000 rpm. When oil flow was stopped to the fluid-film bearing the ball bearing inner race accelerated smoothly and quickly to the shaft speed. When oil flow was restored, the bearing returned to series-hybrid operation.

APPENDIX

DESIGN OPTIMIZATION OF A CONICAL HYDROSTATIC BEARING FOR MINIMUM FRICTION

(Analysis from Ref. 8)

1. Analytical Background

Following the analysis given in the cited reference, the dimensionless thrust load and flow rate are:

$$\overline{F} = X_4^2 + X_3^2 - X_2^2 - 1 \tag{1}$$

$$\overline{Q} = \frac{1}{\ln X_2} + \frac{1}{\ln \frac{X_4}{X_3}} \tag{2}$$

where

$$2\overline{F} = \frac{F}{\pi p R_1^2} \tag{3}$$

$$\overline{Q} = \frac{6\mu Q}{\pi p h_L^3 \sin \theta} \tag{4}$$

$$X_i = \frac{R_i}{R_1} \tag{5}$$

and F is the thrust load, Q the flow rate, p the pocket pressure, h_L the land clearance, μ the fluid viscosity, and θ the half-cone angle (45^o for the present case).

The friction torque M_t consists of the torque M_L due to the laminar shearing of the fluid between inner and outer circumferential lands and the mating surface and the friction torque M_p, resulting from the shearing of the fluid in the bearing pockets which may be laminar or turbulent

depending on the relative rotational speed. M_L can be expressed as,

$$\overline{M}_L = X_4^4 - X_3^4 + X_2^4 - 1 \tag{6}$$

where

$$M_L = \frac{2h_L \sin\theta\, M_L}{\pi\mu(\omega_s - \omega_b)R_1^4} \tag{7}$$

and ω_s is the shaft speed and ω_b the ball bearing speed. The pocket friction $\overline{M}_p$ depends on the Reynolds number defined by

$$R_e = \frac{\rho R_2(\omega_s - \omega_b)hp}{\mu} \tag{8}$$

where h_p is the pocket depth. The expression for the normalized pocket friction torque for laminar flow is

$$\overline{M}_p = C_1\left(X_3^4 - X_2^4\right) \quad \text{for } R_e \leq 1000 \tag{9}$$

where

$$C_1 = 4f_r \frac{h_L}{h_p} \tag{10}$$

and f_r is the fraction of area between R_2 and R_3 occupied by hydrostatic pockets (f_r is close to one for the present case). For turbulent flow, the normalized torque is

$$\overline{M}_p = C_2\left(X_4^{4.75} - X_2^{4.75}\right) \quad \text{for } R_e > 1000 \tag{11}$$

where

$$C_2 = \frac{0.124}{4.75} f_r \left[\rho \frac{R_1(\omega_s - \omega_b)h_p}{\mu}\right]^{0.75} \frac{h_L}{h_p} \tag{12}$$

For given load $\overline{F}$ and flow $\overline{Q}$, values of X_2, X_3, and X_4 that yield a minimum total friction torque $\overline{M}_t$ are given in the reference in graphical form. Actually, X_2, X_3, and X_4 are related through Equations (1) and (2). Therefore, X_2 may be considered as the only dependent variable and, X_3 and X_4 may be expressed in terms of $\overline{F}$, $\overline{Q}$, and X_2 as:

$$X_3^2 = \frac{\overline{F} + X_2^2 + 1}{1 + \exp\left(\dfrac{2}{\overline{Q} - \dfrac{1}{\ln X_2}}\right)} \tag{13}$$

and

$$X_4 = X_3 \exp\left(\frac{1}{\overline{Q} - \dfrac{1}{\ln X_2}}\right) \tag{14}$$

The relationship between the optimal value of X_2 and $\overline{F}$ and $\overline{Q}$ is shown in Fig. 10, which was reproduced from [8].

For a given design load, the value of $\overline{F}$ depends on the level of pocket pressure p (see Eq. (3)). Pocket pressure p, as will be shown later, is a function of the orifice restriction, bearing geometry, and clearance. Thus, for a given design load, the factors affecting pocket pressure have to be established.

For this hydrostatic, fluid-film bearing in the series hybrid bearing system, oil is fed to the bearing pockets centrifugally. The supply pressure is, therefore,

$$p_s = \frac{1}{2} \rho R_0^2 \omega_s^2 \tag{15}$$

where R_0 is the radius defining the location of the feeding orifices. Using Bernoulli's equation, the flow rate through the orifices is

$$Q = C_d n \pi d^2 \frac{1}{4}\left[\frac{2(p_s - p)}{\rho}\right]^{1/2} \tag{16}$$

where n is the number of orifices, d the orifice diameter, ρ the pocket pressure downstream of the orifices, and C_d the orifice discharge coefficient accounting for any deviation from ideal orifice flow. Continuity requires that the orifice flow rate must be equal to the flow rate through the bearing clearance. This requirement gives rise to the expression for the pocket pressure as follows:

$$\bar{p} = \frac{-1 + (1 + 4k^2)^{1/2}}{2k^2} \tag{17}$$

where

$$\bar{p} = \frac{p}{p_s} \tag{18}$$

$$k = \left(\frac{2\rho p_s}{9}\right)^{1/2} \frac{h_L^3 \sin\theta}{C_d n d^2 \mu}\left(\frac{1}{\ln X_2} + \frac{1}{\ln \frac{X_4}{X_3}}\right) \tag{19}$$

k may be considered as the ratio of the orifice flow resistance to the fluid-film flow resistance.

The procedure of using the available data given in [8] to select a bearing configuration for minimum friction is described below.

2. Bearing Configuration Selection Procedure

In order to use the bearing data given in reference [8] effectively, the following scheme has been employed and automated on a digital computer

The selection of the optimized bearing configuration was performed on the basis of minimum friction.

Procedure

1. Set R_1 = 71.1 millimeters (2.81 in.) (the minimum value) for minimum friction.

2. Assume a reasonable R_0 ($R_3 > R_0 > R_2$) so that p_s can be calculated from Eq. (15) by letting ω_s be the design speed of 20 000 rpm.

3. Assume a value of $\bar{p}$ ($0 < \bar{p} < 1$) so that p and $\bar{F}$ corresponding to the design load of 17 800 newtons (4000 lb) can be calculated.

4. Assume a value of X_2 ($1 < X_2 < X_4$ and $X_4 < \frac{3.34}{2.81} = 1.19$). Using the relation among X_2, F and Q given in Fig. 10 ($\bar{Q}$) corresponding to F = 17 800 newtons (4000 lb) is obtained. $\bar{Q}$ as a function of $\bar{F}$ and X_2 is stored in the selection computer program as a two-dimensional numerical table.

5. From ($\bar{F}$), ($\bar{Q}$) and X_2, X_3 and X_4 are obtained from Eqs. (13) and (14).

6. Compute the flow resistance ratio (k) corresponding to F = 17 800 newtons (4000 lb) by using Eq. (17). Then calculate $(h_L)/C_d n d^2$ from Eq. (19).

7. From $\bar{F}$ and F = 4450 newtons (1000 lb), compute the corresponding p and $\bar{p}$.

8. Calculate (k) and $(h_L)^3/C_d n d^2$ similar to step 6.

9. Using Eq. (16) and setting (Q) = 37.9 liters per minute (10 gpm), calculate the maximum value for $C_d n d^2$ to satisfy the flow requirement

10. Let $C_d nd^2$ be equal to the obtained maximum value for minimum friction. Compute (h_L). Thus, the bearing configuration is completely defined for F = 17 800 newtons (4000 lb) and 4450 newtons (1000 lb).

Since the bearing friction torque is approximately proportional to the bearing radius raised to the fourth power or higher (see Eq. (6) and (11)), small bearings yield lower torques. For a given load, a small bearing requires high pocket pressure and from Eq. (3), the corresponding dimensionless load $\overline{F}$ is small. The available optimized bearing data, shown in Fig. 10, only covers $\overline{F}$ from 0.5 to 10. $\overline{F}$ = 0.5 corresponds to $\overline{p}$ = 0.377 (pocket pressure is 37.7 percent of supply pressure). In the bearing configuration selection process, for $\overline{p} > 0.0377$ ($\overline{F} < 0.5$) the optimized bearing configurations were obtained by linear extrapolation of the available data given in Fig. 10.

The bearing clearances at the design load are largest for $\overline{p}$ = 0.3. Because of the high load carrying capacity at off-design conditions and the good performance in terms of stiffness, flow, oil film thickness at design conditions, $a\overline{p}$ = 0.3 was selected for the fluid-film bearing final design.

The selection of the pocket depth h_p involves a compromise between stiffness and torque. High h_p/h_L values exhibit low stiffness and low torque. The inverse holds true for low values of h_p/h_L. High values of h_p/h_L require unrealistically deep pockets while low values increase the operational torque causing unfavorable speed distribution in the final bearing and high power losses. An h_p/h_L of 100 representing an average value was thus selected for this application.

The selected values of $\bar{p}$ and h_p/h_L indirectly established a bearing configuration of the following make-up:

Dimensionless Parameters

$\bar{p}$	0.3
$\bar{Q}$	55.50
$\bar{F}$	0.6189
h_p/h_L	100

Bearing Dimensions

R_0	76.2 mm (3 in.)
R_1	71.4 mm (2.810 in.)
R_2	74.2 mm (2.922 in.)
R_3	81.5 mm (3.210 in.)
R_4	84.3 mm (3.329 in.)
h_p	0.0345 mm (0.136 in.)
$C_d nd^2$	5.26 mm^2 (0.00816 in.)^2
θ	45^o

REFERENCES

1. Coe, H. H., Parker, R. J., and Scibbe, H. W., "Evaluation of Electron-Beam-Welded Hollow Balls for High-Speed Ball Bearings," Journal of Lubrication Technology, Trans. ASME, Vol. 93, Ser. F, Jan. 1971, pp. 47-59.

2. Coe, H. H., Scibbe, H. W., and Anderson, W. J., "Evaluation of Cylindrically Hollow (Drilled) Balls in Ball Bearings at DN Values to 2.1 Million," TN D-7007, NASA, Washington, D.C., 1971.

3. Holmes, P. W., "Evaluation of Drilled-Ball Bearings at DN Values to Three Million. I - Variable Oil Flow Tests," CR-2004, NASA, Washington, D.C., 1972.

4. Holmes, P. W., "Evaluation of Drilled-Ball Bearings at DN Values to Three Million. II - Experimental Skid Study and Endurance Tests," CR-2005, NASA, Washington, D.C., 1972.

5. Scibbe, H. W., and Munson, H. E., "Experimental Evaluation of 150-Millimeter Bore Bearings to 3-Million DN Using Either Solid or Drilled Balls," Journal of Lubrication Technology, Trans. ASME, Series F, Vol. 96, No. 2, April 1974, pp. 230-236.

6. Anderson, W. J., Fleming, D. P., and Parker, R. J., "The Series Hybrid Bearing - A New High-Speed Bearing Concept," Journal of Lubrication Technology, Trans. ASME, Vol. 94, Series F, No. 2, April 1972, pp. 117-124.

7. Nypan, L. J., Scibbe, H. W., and Hamrock, B. J., "Optimal Speed Sharing Characteristics of a Series-Hybrid Bearing, Journal of Lubrication Technology, Trans. ASME, Vol. 95, Series F, No. 1, Jan. 1973, pp. 76-31

8. Nypan, L. J., Hamrock, B. J., Scibbe, H. W., and Anderson, W. J., "Optimization of Conical Hydrostatic Bearing for Minimum Friction," Journal of Lubrication Technology, Trans. ASME, Vol. 94, Series F, No. 2, April 1972, pp. 130-142.

9. Gu, A., Eusepi, M., and Winn, L. W., "Evaluation of a Series Hybrid Thrust Bearing at DN Values to Three Million. I - Analysis and Design," CR-2366, NASA, Washington, D.C., 1974.

10. Eusepi, M., and Winn, L. W., "Evaluation of a Series Hybrid Thrust Bearing at DN Values to Three Million. II - Fabrication and Testing," CR-2542, NASA, Washington, D.C., 1975.

TABLE I. - BALL BEARING TORQUE CHARACTERISTICS

Inner-race speed, rpm	Torque, N-m (in-lb)	
	Axial load, 8900 N (2000 lb)	Axial load, 17 800 N (4000 lb)
6 670	3.72 (32.9)	6.38 (56.5)
10 000	4.66 (41.2)	10.89 (96.4)
13 000	6.27 (55.5)	13.33 (118)
15 200	7.70 (68.1)	13.00 (115)
16 660	8.37 (74.1)	14.57 (129)
18 330	9.10 (80.5)	15.59 (138)
20 000	9.53 (84.3)	17.52 (155)

TABLE II. - DIFFERENTIAL SPEED DATA

Shaft speed, ω_s, rpm	Ball bearing speed, ω_b, rpm	$\frac{\omega_b}{\omega_s}$	Load	
			Newtons	lb
20 000	9 200	0.46	17 800	4000
20 000	12 200	0.61	8 900	2000
15 000	7 200	0.48	17 800	4000
15 000	9 000	0.60	8 900	2000
10 000	5 900	0.59	8 900	2000

TABLE III. - SERIES-HYBRID BEARING EXPERIMENTAL RESULTS

Axial load, N (lb)	Rotor speed, rpm	Oil supply pressure, 10^4 N m^2 (lb in^2)	Oil inlet temperature, °C (°F)	Flow rate, 10^{-4} m^3 sec (gpm)	Film thickness, 10^{-5} m (10^{-3} in.)	$\frac{\omega_b}{\omega_s}$	$\frac{\omega_c}{\omega_b}$	Torque N-m (in-lb)	Power loss, watts (HP)	Ball bearing outer race temperature, °C (°F)	Oil discharge temperature, °C (°F)
4 450 (1000)	5 000	48.3 (70)	93.3 (200)	1.20 (1.90)	2.03 (0.80)	0.480	0.441	1.46 (12.90)	763 (1.02)	98.3 (209)	97.2 (207)
4 450 (1000)	6 000	45.5 (66)	94.4 (202)	1.38 (2.18)	2.11 (0.83)	.470	.450	1.59 (14.06)	998 (1.34)	99.4 (211)	98.9 (210)
4 450 (1000)	7 000	41.4 (60)	95.5 (204)	1.60 (2.53)	2.24 (0.88)	.469	.469	2.06 (18.28)	1514 (2.03)	100 (212)	100 (212)
4 450 (1000)	10 000	31.7 (46)	96.6 (206)	2.68 (4.25)	2.74 (1.08)	.483	.478	4.00 (35.43)	4194 (5.62)	105 (221)	106 (221)
6 620 (1500)	10 000	31.0 (45)	96.6 (206)	2.59 (4.10)	2.74 (1.08)	.473	.507	3.18 (28.20)	3338 (4.47)	106 (222)	106 (222)
8 900 (2000)	10 000	35.8 (52)	96.6 (206)	1.78 (2.82)	1.93 (0.76)	.495	.509	3.38 (29.95)	3545 (4.75)	106 (222)	106 (222)
8 900 (2000)	15 000	12.4 (18)	87.8 (190)	3.85 (6.10)	2.26 (0.89)	.475	.577	5.40 (47.80)	8487 (11.4)	120 (249)	123 (254)
13 350 (3000)	15 000	11.7 (17)	82.8 (181)	3.73 (5.92)	0.66 (0.26)	.507	.567	6.03 (53.40)	9481 (12.7)	122 (251)	101 (214)
13 350 (3000)	15 000	11.6 (16)	85.5 (186)	3.72 (5.90)	0.56 (0.22)	.507	.612	5.97 (52.90)	9392 (12.6)	122 (251)	104 (220)

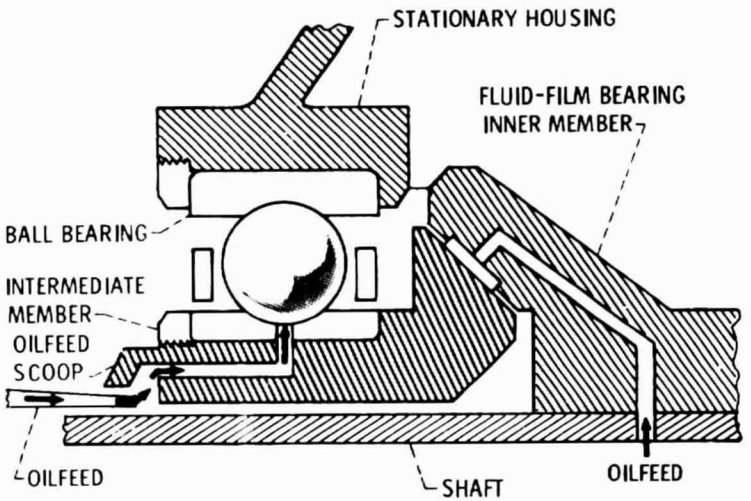

Figure 1. - Schematic diagram of a typical series-hybrid fluid-film, rolling element bearing.

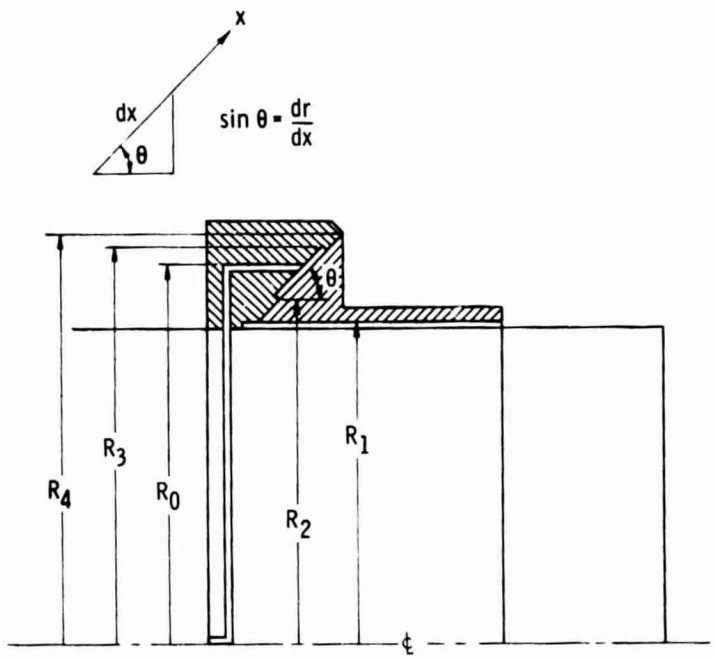

(a) SECTION VIEW.

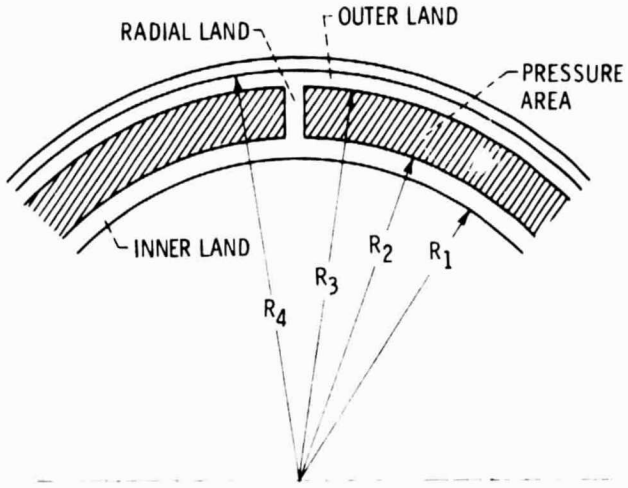

(b) FRONT VIEW.

Figure 2. - Schematic diagrams of conical hydrostatic bearing design.

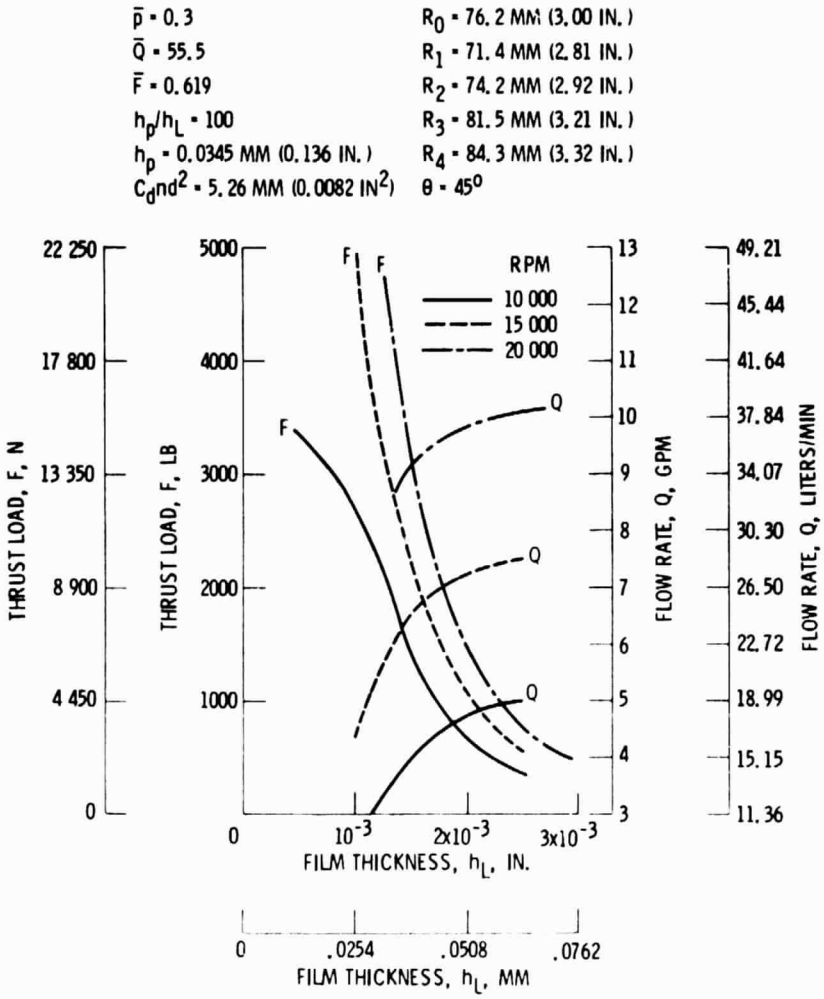

Figure 3. - Load and flow versus film thickness for the selected fluid-film bearing design; design shaft speed of 20 000 rpm and off design shaft speeds of 15 000 and 10 000 rpm.

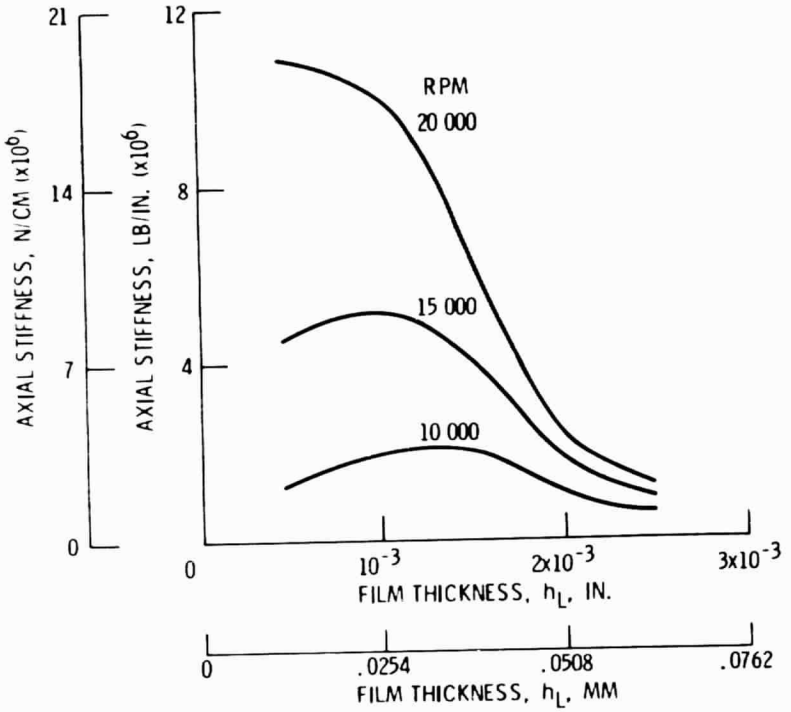

Figure 4. - Axial stiffness of fluid-film bearing versus film thickness for three shaft speeds.

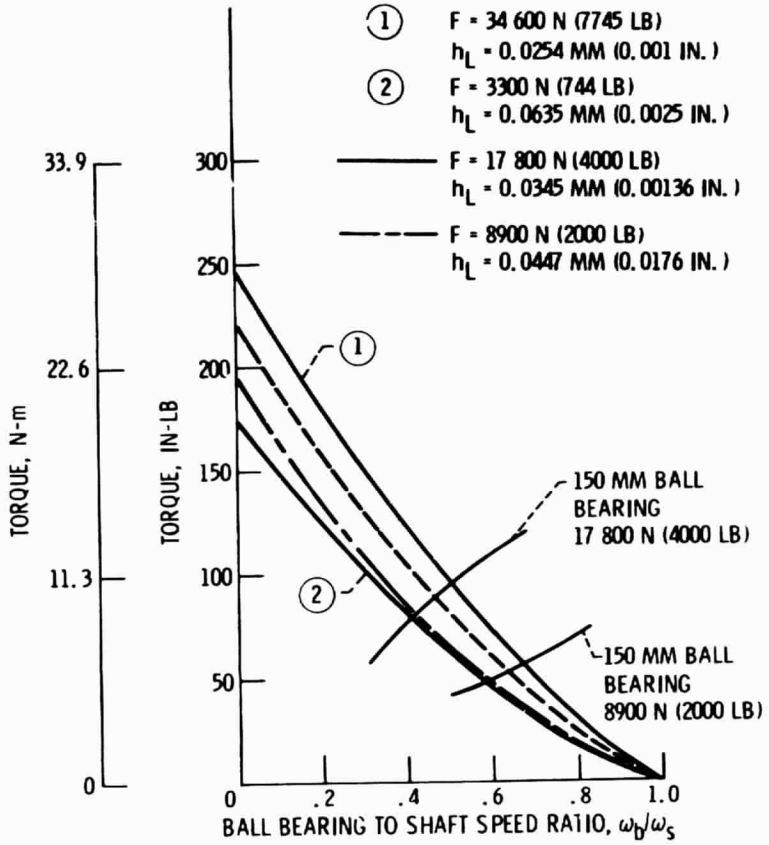

Figure 5. - Torque versus speed ratio, ω_b/ω_s for series-hybrid bearing selected design; 150 mm split inner-ring ball bearing.

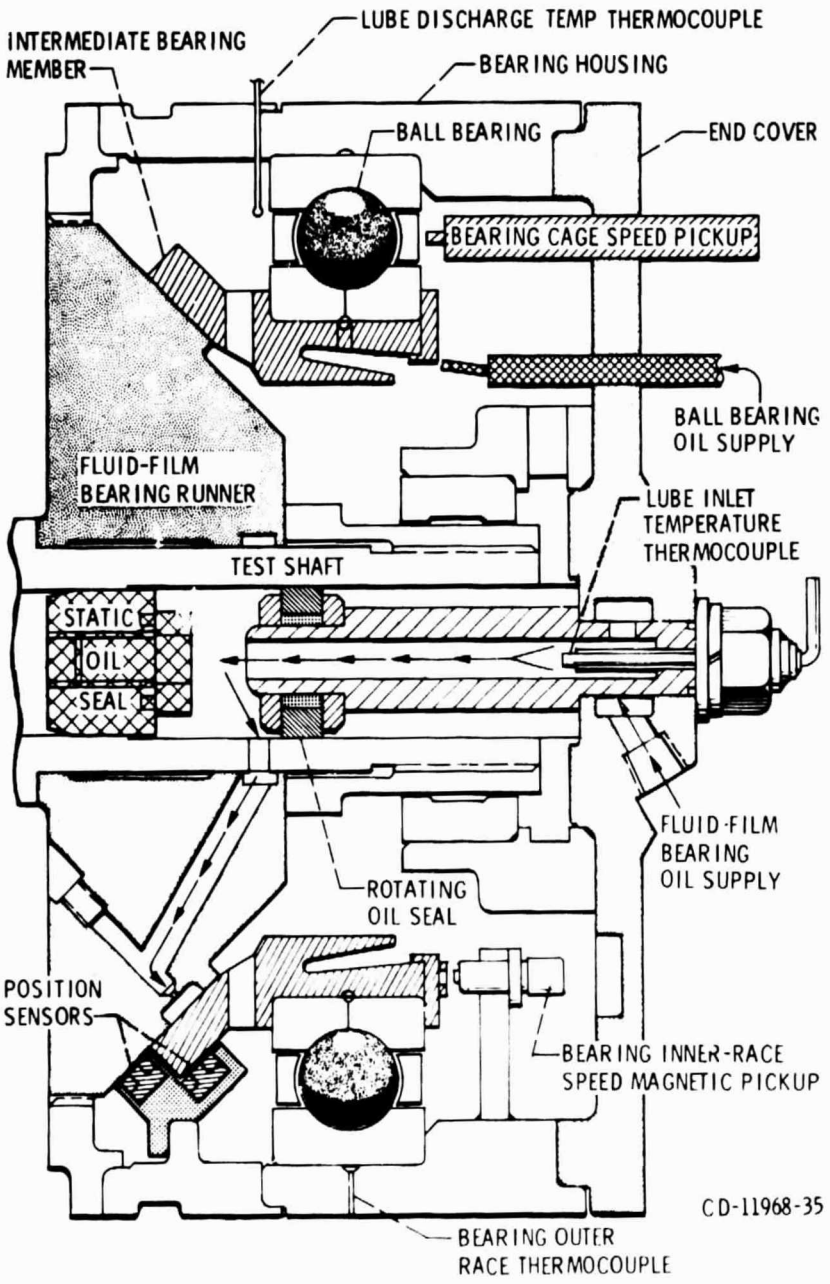

Figure 6. - Schematic of test head assembly.

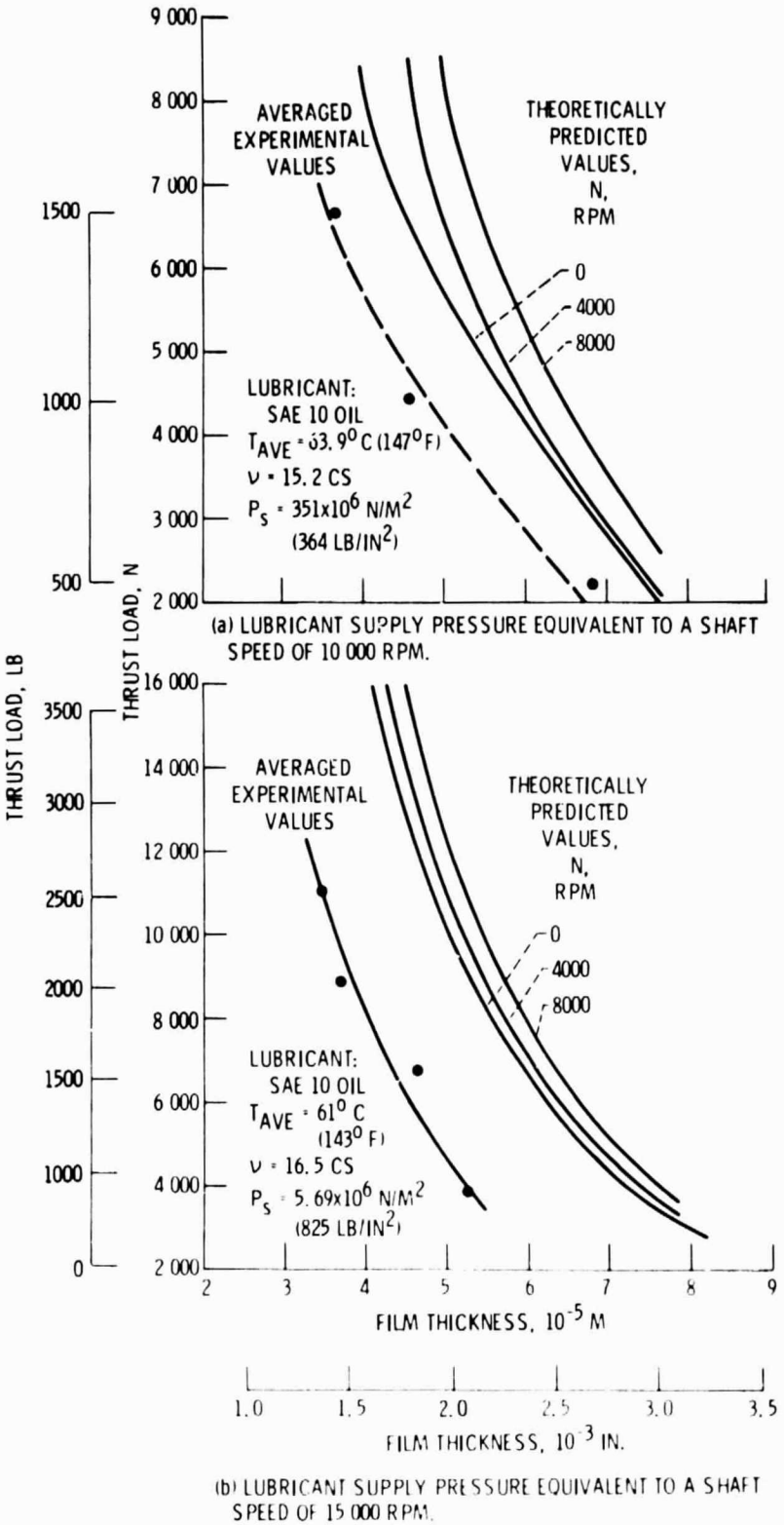

Figure 7. - Fluid-film bearing film thickness as a function of applied thrust load. Comparison between experimental and theoretically predicted values.

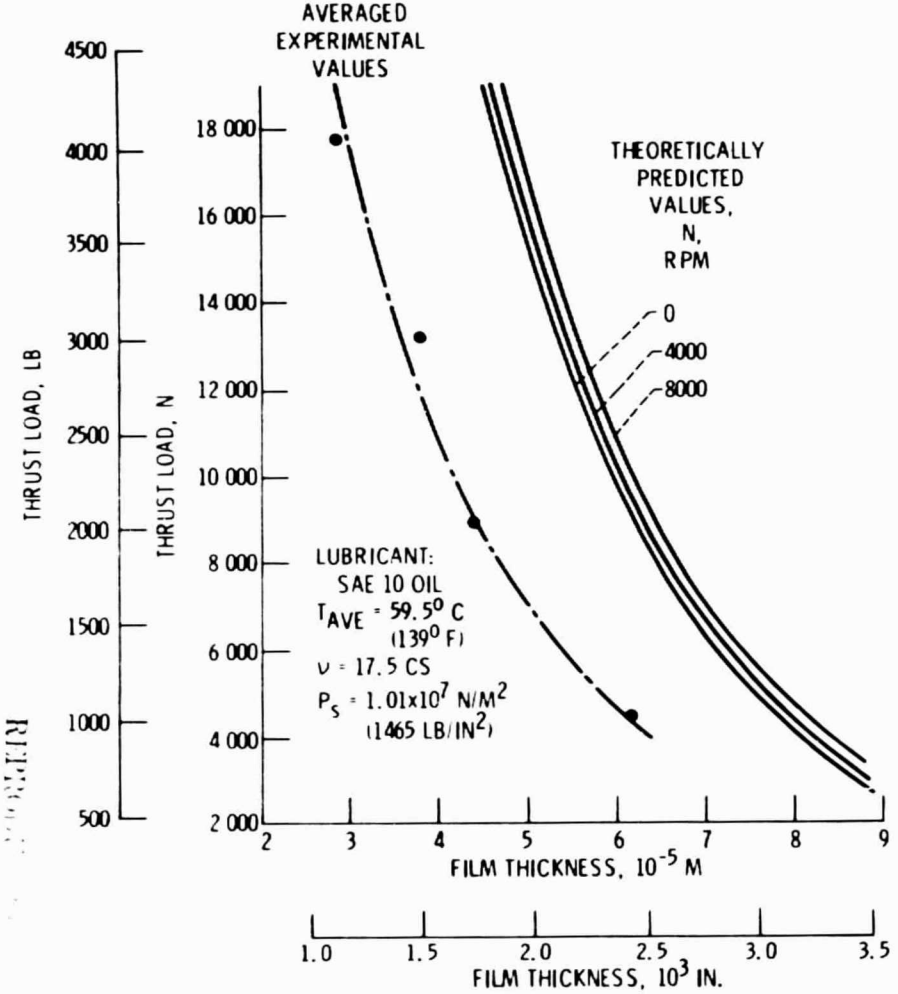

(c) LUBRICANT SUPPLY PRESSURE EQUIVALENT TO A SHAFT SPEED OF 20 000 RPM.

Figure 7. - Concluded.

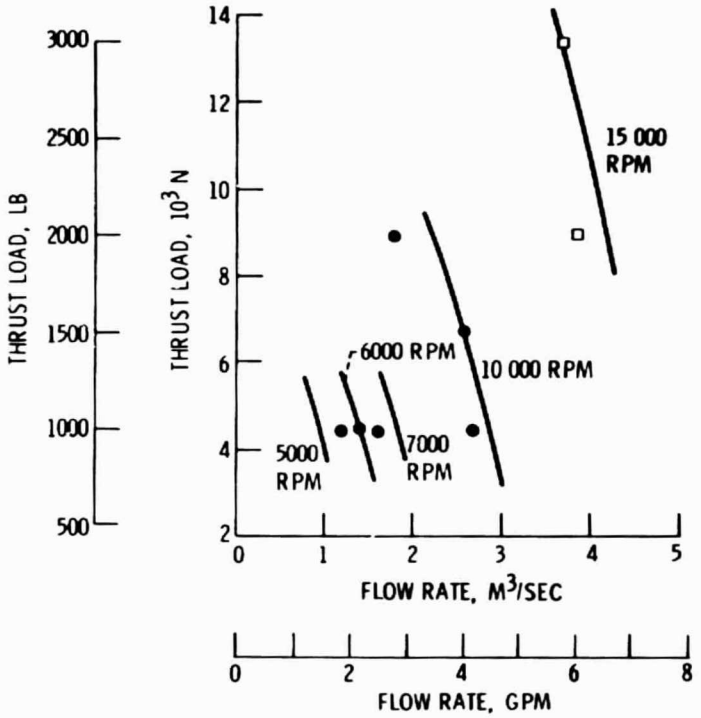

Figure 8. - Experimental test results of the series hybrid bearing. Flow rate as a function of applied thrust load. Lubricant, type II ester (MIL-L-23699) at 367 K (200° F) inlet temperature.

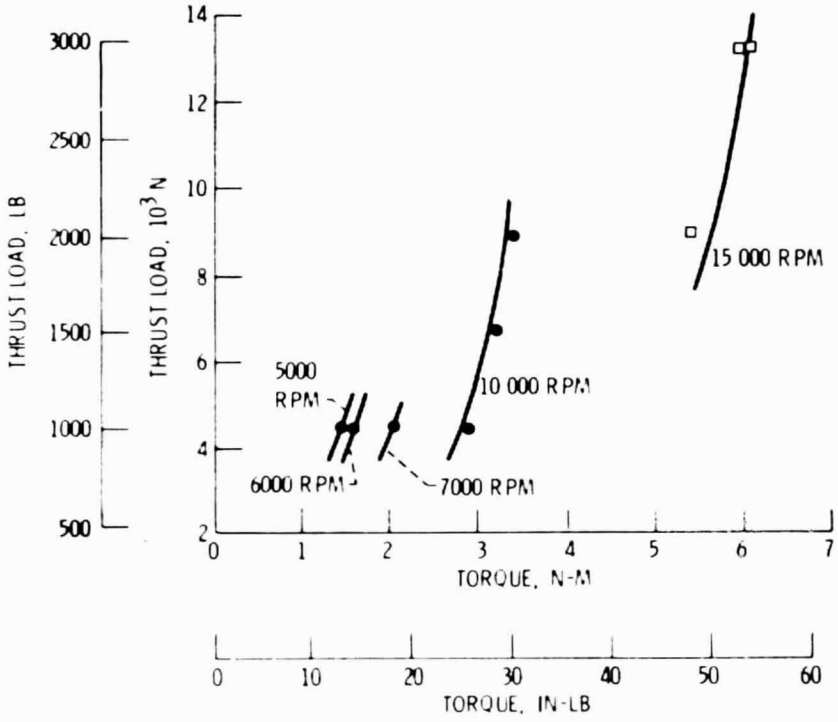

Figure 9. - Experimental test results of the series hybrid bearing. Torque as a function of applied thrust load. Lubricant, type II ester (MIL-L-23699) at 367 K (200° F) inlet temperature.

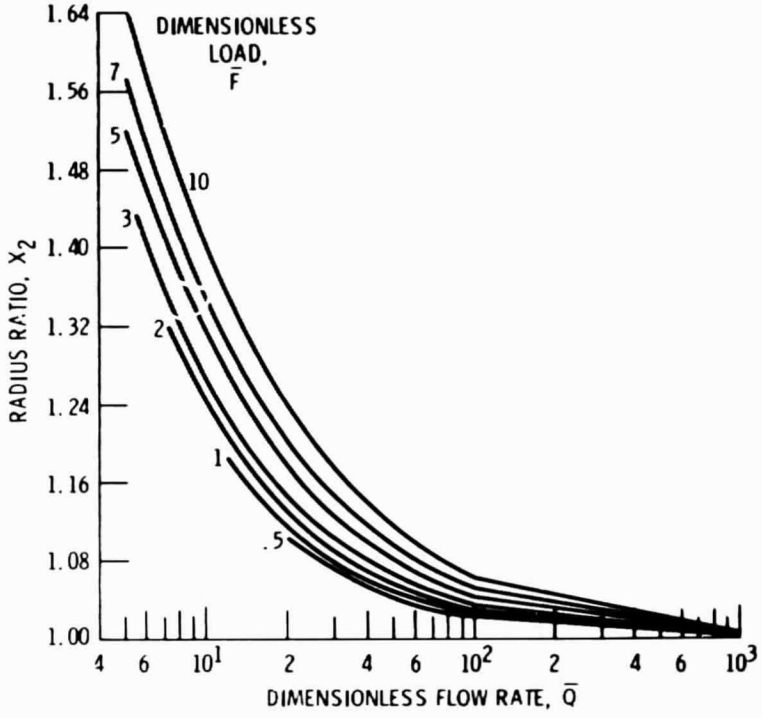

Figure 10. - Effect of flow rate on radius ratio X_2 for optimal bearing. Dimensionless laminar friction coefficient, 0 (from ref. 8).